

Forschungszentrum Karlsruhe
Technik und Umwelt

Wissenschaftliche Berichte
FZKA 5962

Magneto-convection in Long Vertical Rectangular Channels

L. Bühler

Institut für Angewandte Thermo- und Fluidodynamik
Projekt Kernfusion

August 1997

FORSCHUNGSZENTRUM KARLSRUHE
Technik und Umwelt
Wissenschaftliche Berichte
FZKA 5962

Magneto-convection in long vertical rectangular channels

L. Bühler

Institut für Angewandte Thermo- und Fluidodynamik
Projekt Kernfusion

Forschungszentrum Karlsruhe GmbH, Karlsruhe
1997

Als Manuskript gedruckt
Für diesen Bericht behalten wir uns alle Rechte vor
Forschungszentrum Karlsruhe GmbH
Postfach 3640, 76021 Karlsruhe
Mitglied der Hermann von Helmholtz-Gemeinschaft
Deutscher Forschungszentren (HGF)
ISSN 0947-8620

Magneto-convection in long vertical rectangular channels

Abstract

The buoyancy driven laminar magnetohydrodynamic flow in long vertical channels is investigated. It is assumed that the channels have rectangular cross section with one pair of walls aligned with the strong magnetic field. The walls may have arbitrary electrical conductance. Using asymptotic methods, solutions are derived for general temperature distributions inside the ducts. Results are shown for different values of the control parameters. One finds the typical subregions for the flow inside the duct, namely the inviscid core, surrounded by viscous Hartmann layers and side layers. The character of the solution inside these regions may deviate from what is expected by a comparison with the classical solutions for pressure driven duct flows. The main difference is that the flow in the core not necessarily exhibits a two-dimensional behavior. Most surprising, however, is the fact, that high-velocity jets are observed for the first time along perfectly conducting side walls. These jets are able to carry a major part of the flow rate.

MHD Konvektion in langen vertikalen rechteckigen Kanälen

Zusammenfassung

In diesem Bericht werden magnetohydrodynamische Strömungen untersucht, die durch thermische Auftriebskräfte hervorgerufen werden. Es wird vorausgesetzt, daß die Kanäle einen rechteckigen Querschnitt aufweisen, wobei jeweils zwei Wände parallel zum Magnetfeld angeordnet sind. Mittels asymptotischer Verfahren werden Lösungen für allgemeine Temperaturverteilungen hergeleitet. Die Ergebnisse werden für verschiedene Werte der Kontrollparameter vorgestellt. Man findet die typischen Strömungsgebiete im Kanal, nämlich den reibungsfreien Strömungskern, der von viskosen Hartmann- und Seitenschichten umgeben ist. Verglichen mit klassischen druckgetriebenen Kanalströmungen ergeben sich hier unerwartete Lösungen. Der Hauptunterschied ist, daß der Strömungskern nicht notwendigerweise ein zweidimensionales Verhalten aufweist. Überraschend ist vor allem die Tatsache, daß erstmals Jets mit hohen Geschwindigkeiten entlang von perfekt leitenden Wänden auftreten, die einen erheblichen Anteil des Volumenstroms fördern.

Magneto-convection in long vertical rectangular channels

L. Bühler

Contents

1	Introduction	3
2	Formulation	5
2.1	Basic equations	5
2.2	Simplifications	7
3	Analysis	10
3.1	Core solution	10
3.2	Hartmann layers	11
3.3	Implications on the core solution	11
3.4	Side layers	12
4	Applications	15
4.1	Isothermal flows	15
4.2	Heat flux perpendicular to \mathbf{B}	16
4.2.1	y -symmetric case	16
4.2.2	Non y -symmetric case	19
4.3	Heat flux aligned with \mathbf{B}	23
5	Conclusions	28
	References	30

1 Introduction

In currently investigated liquid-metal (LM) blankets for fusion reactors the liquid metal serves mainly as breeding material. The high fusion heat flux is removed from the blanket and from the plasma by separate cooling devices. This has some advantage in comparison to the self-cooled LM concepts where high velocities are required to remove the fusion heat by the LM-coolant. While in self-cooled blankets a high pressure head drives a forced flow which is very strong compared to buoyant effects, this is not the case for the separately cooled LM-breeder concepts. It may happen that the flow induced by non-uniform thermal conditions now is the dominant one in the whole blanket element since the velocities caused by the forced flow are on the scale of a few millimeters per second.

Within the scope of separately cooled LM-breeding blankets the buoyancy driven laminar flow of an electrically conducting fluid in very long vertical channels is investigated. It is assumed that the channels have rectangular cross section with one pair of walls aligned with the strong magnetic field, applied horizontally for the plasma confinement.

A review of buoyant convective MHD flows is given in the text book by Blüms, Mikhailov and Ozols (1987). The example which is most closely related with the present work is the flow confined in a vertical channel formed by two electrically insulating plates of infinite extension. The magnetic field is perpendicular to these plates. The results, originally obtained by Gershuni & Zhukovitskii (1958, published in russian, cited by Blüms et al. (1987)) show that the velocity scales with Gr/M^2 where Gr and M are the Grashof and the Hartmann number, describing the intensity of the buoyant forcing and the magnetic damping, respectively. For definition of these numbers see the next section. The stability of this basic laminar solution has been analyzed by Takashima (1994). He finds for small Prandtl numbers, typical for liquid metals, that the laminar unidirectional flow becomes unstable at critical values of the Grashof number Gr_c . The flow is strongly stabilized with higher intensity of the magnetic field. Increasing the Hartmann number by a factor of four to $M = 8$ increases Gr_c by three orders of magnitude. Unfortunately Takashima does not give results for the parameters focussed in the present paper, where M may reach values of $10^3 - 10^4$ but it can be estimated that the laminar flow may remain stable for Hartmann numbers typical for fusion applications.

The academic problem of a flow between two vertical walls is extended in the present paper by introducing finite dimensions of the duct's cross section, as required in engineering applications. The walls are assumed to be thin, but they may have arbitrary electrical conductance. The temperature inside the ducts may take any value depending on internal heating and/or thermal boundary conditions. The direction of the heat flux is no longer restricted to the direction of the magnetic field as was assumed in the works cited above. It is further supposed that the flow remains laminar. Using asymptotic methods, solutions are derived for general temperature distributions inside the ducts. Results are shown for different values of the control parameters. One finds the typical subregions for the flow inside the duct, namely the inviscid core, surrounded by viscous Hartmann layers and side layers. It will be shown that character of the solution inside these regions may deviate from what is expected by a comparison with the classical

solutions for pressure driven duct flows. The main difference is that the flow in the core not necessarily exhibits a two-dimensional behavior. Most surprising, however, is the fact, that high-velocity jets are observed for the first time along perfectly conducting side walls. These jets are able to carry a major part of the flow rate.

Magnetoconvective flows have been analyzed in the past for a number of other different geometries. Moreau and coworkers Garandet, Alboussière and Moreau (1992), Alboussière, Garandet and Moreau (1993) as well as Ben Hadid, Henri and Kaddeche (1997), consider the case of a horizontal Bridgman configuration for crystal growth, while Walker and co-authors focus on the cylindrical geometry typical for the Czochralski crystal puller Hjellming and Walker (1987), Hjellming, Tolley and Walker (1993), Khine and Walker (1994), Ma and Walker (1995), Ma and Walker (1996a), Ma and Walker (1996b). All cited references are using analytical methods of solution. They are all somehow related with applications in crystal growth. The fully numerical approach of Mößner (1996) and may be that of Ben Hadid and Henri (1997) should be considered more as basic research in this field with no direct applications. The most general formulation of the problem of magnetoconvective flows may be found in the paper by Alboussière, Garandet and Moreau (1996).

2 Formulation

The problem considered in this paper is the flow which is caused by buoyancy in long vertical channels of rectangular cross section. The electrically conducting fluid is subjected to a strong, externally applied uniform magnetic field $\mathbf{B} = B\hat{\mathbf{y}}$, parallel to one (or two, if the cavity is closed) pair(s) of walls called the *side walls* of the duct. The gravitational acceleration $\mathbf{g} = -g\hat{\mathbf{x}}$ is aligned with the channels axis (see figure 1).

2.1 Basic equations

The stationary inductionless flow is governed by the equation of motion

$$\frac{Gr}{M^4} (\mathbf{v} \cdot \nabla) \mathbf{v} = -\nabla p + \frac{1}{M^2} \nabla^2 \mathbf{v} + \mathbf{j} \times \hat{\mathbf{y}} + T\hat{\mathbf{x}}, \quad (1)$$

and the conservation of mass

$$\nabla \cdot \mathbf{v} = 0. \quad (2)$$

Here, $\mathbf{v} = (u, v, w)$ and $\mathbf{j} = (j_x, j_y, j_z)$ denote the velocity and the electric current density, scaled by the reference quantities $v_0 = \rho_0 \beta g \Delta T / \sigma B^2$ and $j_0 = \sigma v_0 B$. T represents the difference between a the local temperature and a reference temperature T_0 , scaled by a characteristic temperature difference ΔT . The density of the fluid at temperature T_0 is ρ_0 , the thermal expansion coefficient according to the *Boussinesq approximation* is β . The difference between the local pressure and the isothermal hydrostatic pressure (at T_0) scaled by $Lj_0 B$ is called p . The electric conductivity of the fluid is σ and L stands for a typical length scale measured in the direction of the magnetic field.

The non-dimensional parameters are the

$$\text{Hartmann number } M = LB\sqrt{\sigma/\rho_0\nu} \quad (3)$$

and the

$$\text{Grashof number } Gr = \beta g \Delta T L^3 / \nu^2. \quad (4)$$

The kinematic viscosity is denoted by ν . The square of the Hartmann number gives the ratio of electromagnetic to viscous forces. The Grashof number quantifies the importance of buoyant effects. The velocity scale is given by the viscous scale ν/L times Gr/M^2 , where the ratio Gr/M^2 corresponds to a Reynolds number. The ratio M^4/Gr is often called the interaction parameter.

The current density is obtained by solving Ohm's law

$$\mathbf{j} = -\nabla\phi + \mathbf{v} \times \hat{\mathbf{y}}, \quad (5)$$

with conservation of electric charge

$$\nabla \cdot \mathbf{j} = 0. \quad (6)$$

The variable ϕ is the electric potential, scaled by $Lv_0 B$. Equations similar to those displayed above have been used e.g. by Ma and Walker (1995), Ma and Walker (1996a) for calculations of magneto-convection during Czochralski crystal growth applications,

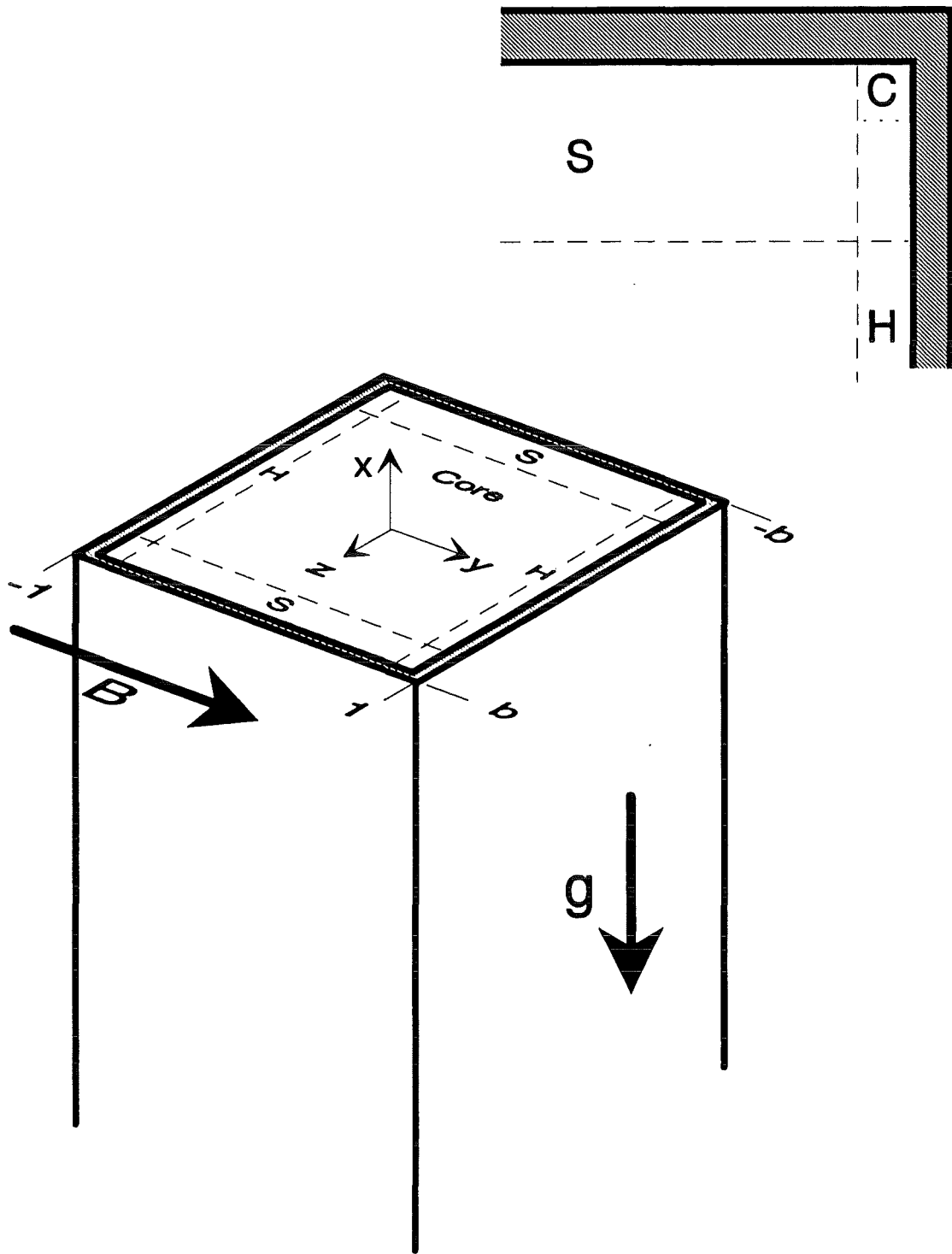


Figure 1: Sketch of the channel geometry. The flow exhibits a core in which viscous forces are negligible. The core is surrounded by the Hartmann layers (H) and by the side layers (S) at walls perpendicular and parallel to the magnetic field \mathbf{B} . The corner regions are indicated by (C).

while e.g. Alboussière et al. (1993), Alboussière et al. (1996), Mößner (1996), Ben Hadid and Henri (1997) prefer scales different from these.

The temperature distribution is governed by an energy balance

$$Pe(\mathbf{v} \cdot \nabla)T = \nabla^2 T + Q. \quad (7)$$

The quantity Q is the volumetric heat source scaled by $\lambda\Delta T/L^2$, caused e.g. by viscous or Ohmic dissipation or due to nuclear irradiation. The thermal conductivity of the fluid is λ . The

$$Peclet\ number\ Pe = v_0 L / \kappa \quad (8)$$

gives the ratio of convective to conductive heat flux. The thermal diffusivity is denoted by κ .

The boundary conditions are the no-slip condition at the duct walls

$$\mathbf{v} = 0, \quad (9)$$

and the *thin wall condition* for electric currents

$$\mathbf{j} \cdot \mathbf{n} = c \nabla_w^2 \phi. \quad (10)$$

The subscript ' $_w$ ' denotes properties at the wall and ∇_w^2 is the two-dimensional Laplacian in the plane of the wall. The constant c is called the

$$wall\ conductance\ ratio\ c = \sigma_w t. \quad (11)$$

The ratio of the electric wall to fluid conductivity is σ_w . The non-dimensional thickness of the wall t is assumed to be small, $t \ll 1$. Equation (10) ensures charge conservation in the plane of the wall; currents leaving the fluid enter the wall balance as a source term and create inside the wall a potential distribution. It is further assumed that there is no contact resistance at the fluid wall interface so that the fluid potential ϕ at the wall is equal to the wall potential. Note, \mathbf{n} is the *inward* unit normal to the duct wall.

The thermal conditions are

$$T = T_w \quad \text{or} \quad \mathbf{n} \cdot \nabla T = -q_w \quad (12)$$

for perfectly thermally conducting walls or for a given non-dimensional wall heat flux q_w .

2.2 Simplifications

The fluids under consideration are assumed to have excellent heat conduction. This assumption is fairly valid for liquid metals or semiconductors and leads to great simplifications for the further analysis. With this assumption the convective heat flux is negligible if $Pe \ll 1$. The temperature distribution becomes independent of the flow and can be calculated in a first step by solving $\nabla^2 T = -Q$ with the corresponding thermal boundary conditions.

It is further assumed that the Hartmann number is sufficiently large, e.g.

$$M^4 \gg Gr \quad (13)$$

so that inertia effects can be neglected in the momentum balance. It is known, that at duct walls which are parallel to the applied magnetic field (here the y - direction) high-velocity jets with $|\mathbf{v}| \sim \sqrt{M}$ may occur. Velocities larger than $O(1)$ are further possible for a poor conductivity of the duct walls. If this is the case, the above criteria has to be reconsidered. Then, $M^4 \gg Gr(\mathbf{v} \cdot \nabla)\mathbf{v}$ is the restriction for inertia terms to be negligibly small. For application in fusion engineering M reaches values of 10^3 - 10^4 so that the criterium for inertialess flow is satisfied in most cases. The simplified equations now read:

$$\nabla p = \frac{1}{M^2} \nabla^2 \mathbf{v} + \mathbf{j} \times \hat{\mathbf{y}} + T \hat{\mathbf{x}}, \quad (14)$$

$$\nabla \cdot \mathbf{v} = 0 \quad (15)$$

$$\mathbf{j} = -\nabla \phi + \mathbf{v} \times \hat{\mathbf{y}}, \quad (16)$$

$$\nabla \cdot \mathbf{j} = 0. \quad (17)$$

The boundary conditions are not affected by the simplifications.

For very high values of M the flow region splits into several distinct regions. The major part of the fluid domain is occupied by the core, in which viscous effects are negligible. In the core, the momentum is balanced between the pressure gradient ∇p , the Lorentz force $\mathbf{j} \times \hat{\mathbf{y}}$, and the buoyant force $T \hat{\mathbf{x}}$. Viscous effects become important within the near-wall boundary layers. The viscous layers near $y = \pm 1$, which are perpendicular to the applied magnetic field, are called the *Hartmann layers*. Their thickness scales with M^{-1} . The Hartmann layers match exponentially the core solution with the no-slip condition at so-called *Hartmann walls*. The layers at $z = \pm b$ are called the *side layers*. Their thickness is $M^{-1/2}$. It is well known from a number of classical papers about pressure driven MHD duct flows that the side layers are capable (under certain circumstances) to carry a significant fraction of the total flow rate. The portion of flow carried by the side layers depends essentially on the conductivity of the side wall $c = c_S$. For highly conducting side walls, $c_S = \infty$, no volume flux is carried by the layer. However, if the conductivity is finite, especially if $c_S \ll 1$, the flow carried by the side layer reaches a magnitude of order one. This leads to high velocity jets with velocities on the scale of $M^{1/2}$.

The equations displayed above describe the problem completely. For the further analysis it is useful to introduce the vorticity $\boldsymbol{\omega} = (\omega_x, \omega_y, \omega_z)$

$$\boldsymbol{\omega} = \nabla \times \mathbf{v}, \quad (18)$$

and to use equations derived from the basic conservation laws. With this notation the conservation of charge (17) together with Ohm's law (16) gives a relation between the y -component of vorticity and the electric potential

$$\nabla^2 \phi = \omega \cdot \hat{\mathbf{y}}. \quad (19)$$

Taking the curl of the momentum equation eliminates the pressure and yields

$$\frac{1}{M^2} \nabla^2 \boldsymbol{\omega} + \partial_y \mathbf{j} - \hat{\mathbf{x}} \times \nabla T = 0. \quad (20)$$

For the further analysis all variables are replaced by their core values plus additional viscous corrections.

$$\begin{bmatrix} \mathbf{v} \\ \mathbf{j} \\ \boldsymbol{\omega} \\ p \\ \phi \\ T \end{bmatrix} \rightarrow \begin{bmatrix} \mathbf{v} \\ \mathbf{j} \\ \boldsymbol{\omega} \\ p \\ \phi \\ T \end{bmatrix} + \begin{bmatrix} \mathbf{v}_h \\ \mathbf{j}_h \\ \boldsymbol{\omega}_h \end{bmatrix} + \begin{bmatrix} \mathbf{v}_s \\ \mathbf{j}_s \\ \boldsymbol{\omega}_s \\ p_s \\ \phi_s \end{bmatrix} \quad (21)$$

The subscripts ' $_h$ ' and ' $_s$ ' denote the viscous corrections to the core solution in the Hartmann layers and in the side layers, respectively. To avoid a mass of subscripts the core variables are not explicitly denoted by a special index. If subscripts with capital letters ' $_H$ ' or ' $_S$ ' are used, they indicate that the value is taken at the Hartmann or at the side wall. It is well known that across the Hartmann layers the pressure and the potential do not vary, $p_h = \phi_h = 0$ in the leading order of approximation. While the core values depend on the coordinates (x, y, z) , the viscous corrections in the Hartmann layers and in the side layers depend on a stretched wall normal coordinate η and ζ , respectively. These coordinates are defined during the following chapters. Their scale is motivated by the corresponding boundary layer thickness.

3 Analysis

The analysis is performed, using matched asymptotics. In a first step the core solution is obtained. In a second step the core solution is matched with the solution in the Hartmann layers. Finally, the solution in the side layers is calculated.

3.1 Core solution

Considering the vorticity equation (20) in the outer limit as $M \rightarrow \infty$ gives

$$\partial_y j_x = 0, \quad \partial_y j_y = -\partial_z T, \quad \partial_y j_z = \partial_y T. \quad (22)$$

Combining the second of these with the second component of Ohms law (16) leads to

$$\partial_{yy}\phi = \partial_z T. \quad (23)$$

The integration along magnetic field lines gives the potential distribution inside the fluid

$$\phi = \phi_H + \partial_z \tilde{T}, \quad (24)$$

where

$$\tilde{T}(x, y, z) = \frac{1}{2} \left(\int_{-1}^y \int_0^{y_1} T(x, y_2, z) dy_2 dy_1 - \int_y^1 \int_0^{y_1} T(x, y_2, z) dy_2 dy_1 \right). \quad (25)$$

has been introduced for convenient notation. The tilde "˜" above a variable denotes the integration of the variable according to the equation (25). The part of the potential ϕ_H , which is purely dominated by the solution at the Hartmann walls is

$$\phi_H = \frac{1}{2} (1 + y) \phi_+ + \frac{1}{2} (1 - y) \phi_- \quad (26)$$

with the new integration functions ϕ_+ and ϕ_- , the potential at the front and at the rear Hartmann walls, at $y = 1$ and $y = -1$, respectively. The first part gives the average potential due to the Hartmann solution, the second part results from currents along field lines which are exchanged between the Hartmann walls. Note, ϕ_H is not constant along y with this definition. Equation (24) determines the solution within the fluid, supposing that the potentials at the Hartmann walls are known. For the y -symmetric case $\phi_H = \phi_+ = \phi_-$.

The y - component of vorticity is obtained by introducing equation (24) in the equation (19).

$$\omega_y = \nabla_{\perp}^2 \phi_H + \partial_z \nabla^2 \tilde{T}. \quad (27)$$

The symbol ∇_{\perp}^2 stands for the two-dimensional Laplacian in the plane perpendicular to the magnetic field, at $y = \text{const}$. With the energy equation the vorticity component ω_y becomes

$$\omega_y = \nabla_{\perp}^2 \phi_H - \partial_z \tilde{Q}. \quad (28)$$

The y - component of vorticity is determined by the solution at the Hartmann walls alone, if either there is no volumetric heat source or if the volumetric heating is uniform along z .

3.2 Hartmann layers

Within the Hartmann layer a stretched coordinate $\eta = M(1 - y)$ is introduced (here at the wall $y = 1$). Inserting this scale into the vorticity equation (20) yields the ordinary differential equation for the y - component

$$\partial_{\eta\eta}\omega_{yh} - \omega_{yh} = 0 \quad (29)$$

by considering the inner limit as $M \rightarrow \infty$. With the no-slip condition the solution becomes

$$\omega_{yh} = -\omega_y e^{-\eta}, \text{ at } y = 1 \quad (30)$$

The viscous correction vanishes towards the core as $\eta \rightarrow \infty$, but ensures no-slip at the Hartmann wall at $\eta = 0$. Similar relations can be derived for the velocity components parallel to the wall

$$u_h = -ue^{-\eta}, \quad w_h = -we^{-\eta} \text{ at } y = 1. \quad (31)$$

Integrating the vorticity equation (20) along y and considering the inner limit as $M \rightarrow \infty$ gives

$$\partial_{\eta}\omega_{yh} + Mj_{yh} = 0, \text{ at } \eta = 0. \quad (32)$$

Note, Mj_{yh} is $O(1)$ for a reasonable balance of charge according to equation (17). Using the equations (30,19,23), the equation determining the wall potential becomes

$$(c_{\pm} + M^{-1})\nabla_{\perp}^2\phi_{\pm} = \pm\partial_y\phi, \text{ at } y = \pm 1, \quad (33)$$

where ϕ is used according to equation (24). The subscripts denoting the walls become '+' and '-', the sign at the right-hand side + and -, for the front wall and for the rear wall, at $y = 1$ and at $y = -1$, respectively. The new parameter $C_{\pm} = M^{-1} + c_{\pm}$ measures the total conductance of the Hartmann walls and of the Hartmann layers. For the non-symmetric case the equation has to be evaluated at both Hartmann walls separately.

$$C_{\pm}\nabla_{\perp}^2\phi_{\pm} = \pm\frac{1}{2}(\phi_{\pm} - \phi_{\mp}) + \partial_z\bar{T} \text{ at } y = \pm 1. \quad (34)$$

Here and in the following variables with an over-bar like \bar{T} denote average values along y . For the symmetric case the equation determining ϕ_H becomes with $C_+ = C_- = C_H$,

$$\underline{\nabla_{\perp}^2\phi_H = C_H^{-1}\partial_z\bar{T}}_{y\text{-symmetric}}. \quad (35)$$

3.3 Implications on the core solution

With the equation (35) it is now possible to eliminate ϕ_H from the equation (28) and the vorticity component in the core, ω_y , is determined by the temperature field only as

$$\underline{\omega_y = \partial_z(C_H^{-1}\bar{T} - \tilde{Q})}_{y\text{-symmetric}}. \quad (36)$$

This equation shows the following two interesting limits: If the Hartmann walls are poor conducting, $C_H \ll 1$ the first term on the right-hand side is dominant. The vorticity is determined by the y - average temperature. There is no variation of ω_y along magnetic

field lines; the vorticity in the core is strictly two-dimensional even if the temperature field is three-dimensional. This result is not surprising. It corresponds with the well known fact that the core variables do not vary along magnetic field lines as observed in many pressure driven duct flows. More interesting, however, is the second limit, $C_H \gg 1$. For well conducting Hartmann walls the vorticity component is $\omega_y = \partial_z \nabla^2 \tilde{T}$. It turns out that even if T does not vary along y the vorticity can (remember that \tilde{T} has been obtained from T via two integrations along y), especially if the volumetric heat release $Q = -\nabla^2 T$ depends on z .

The velocity distribution is obtained not by an integration of the vorticity field but by considering the Ohm's law. For the z - component,

$$j_z = -\partial_z \phi + u, \quad (37)$$

the current j_z is replaced using the momentum equation in the x - direction

$$\partial_x p = -j_z + T. \quad (38)$$

The potential is eliminated with the help of equation (24) and the velocity component u becomes

$$u = -\partial_x p + T + \partial_{zz} \tilde{T} + \partial_z \phi_H. \quad (39)$$

The z - component of velocity w follows in an analog way

$$w = -\partial_z p - \partial_{xz} \tilde{T} - \partial_x \phi_H. \quad (40)$$

For the y -symmetric case, the velocity components in the plane perpendicular to the magnetic field are composed by two-dimensional parts $-\partial_x p + \partial_z \phi_H$ or $-\partial_z p - \partial_x \phi_H$ analog to pressure driven duct flows (there are no variations along y). In an inhomogeneous temperature field there are additional contributions, $T + \partial_{zz} \tilde{T}$ or $-\partial_{xz} \tilde{T}$ which now can cause variations of u and w along y . Even if the temperature is constant along y the function \tilde{T} and therefore the velocity exhibits a profile in this direction. For the non-symmetric case ϕ_H is a linear function along y .

Using the velocity components given by equations (39,40) in the equation for conservation of mass, integrating along y , knowing that p does not vary along the integration path, leads to equation

$$\nabla_{\perp}^2 p = \partial_x \tilde{T}. \quad (41)$$

This equation determines the pressure in the core. It is the same equation as for the flow in a porous medium. The pressure becomes independent of any fluid motion. It is simply given by the thermal stratification. Boundary conditions for pressure can be obtained from the equations (39,40) by integration along y . Note, the core velocity components u and w normal to the walls are not zero in general, since there may be an exchange of mass between the core and the neighboring side layers. The determination of their integral values requires the detailed consideration of the side layer solution.

3.4 Side layers

Side layers occur near walls which are aligned with the magnetic field. Their thickness is $O(M^{-1/2})$. This scale is known from a number of papers about MHD duct flows and

is therefore not explicitly derived here. With this knowledge the stretched side layer coordinate becomes

$$\zeta = M^{1/2} (b - z), \quad (42)$$

here, as an example for the right side layer at $z = b$. The inner limit of the vorticity equation (20) as $M \rightarrow \infty$ leads to

$$M^{-1} \partial_{\zeta\zeta} \omega_{ys} + \partial_y j_{ys} = 0. \quad (43)$$

Using the equation (19), $M \partial_{\zeta\zeta} \phi_s = \omega_{ys}$, and replacing j_{ys} by $-\partial_y \phi_s$ according to Ohm's law one finds the equation determining the potential in the side layers

$$\partial_{\zeta}^4 \phi_s = \partial_{yy} \phi_s. \quad (44)$$

This result confirms the proper scale for the side layer thickness as assumed just above. The boundary conditions for this equation are the following: If the Hartmann walls are highly conducting, the side layer solution will not affect the potential at the Hartmann walls. $\phi_s = 0$ at $y = \pm 1$. Towards the core the solution has to match asymptotically the core potential, $\phi_s = \partial_{\zeta} \phi_s = 0$ as $\zeta \rightarrow \infty$. At the side wall the potential is equal to the wall potential, $\phi + \phi_s = \phi_S$ at $\zeta = 0$. The condition $\partial_{\zeta} \phi_s = -M^{-1/2} u$ at $\zeta = 0$, $z = b$ ensures no slip at the side wall. This relation is valid if the side wall is much better conducting than the side layer, $c_S \gg M^{-1/2}$. If this is the case, the core currents can pass through the side layer almost unchanged before they reach the side wall ($j_{zs} \ll 1$).

The general solution for ϕ_s which satisfies the boundary condition at the Hartmann walls and the matching condition towards the core is

$$\phi_s = \sum (A_k \cos(\alpha_k \zeta) + B_k \sin(\alpha_k \zeta)) e^{-\alpha_k \zeta} H_k(\beta_k y), \quad (45)$$

with

$$\beta_k = \frac{1}{2} k \pi \text{ and } \alpha_k = \sqrt{\beta_k / 2}. \quad (46)$$

The function $H_k(\beta_k y)$ represents the harmonic functions $\sin(\beta_k y)$ and $\cos(\beta_k y)$, if either k is even or odd. The coefficients are obtained by applying the boundary conditions at $\zeta = 0$.

$$\sum A_k H_k(\beta_k y) = \phi_S - \phi = \phi_s. \quad (47)$$

$$\sum \alpha_k (A_k - B_k) H_k(\beta_k y) = M^{-1/2} u \quad (48)$$

The A_k are the Fourier coefficients of the difference between the side wall and the core potential, the values $\alpha_k (A_k - B_k)$ are the Fourier coefficients of $M^{-1/2}$ times the core velocity u . The relations above are derived here for one side wall at $z = b$. Similar expressions can be obtained for the other side walls as well.

The flow rate carried by the side layer is obtained via an integration of Ohm's law across the layer thickness. The integral flow rate in the layer $U_s(x, y, z = \pm b)$ is defined as

$$U_s = M^{-1/2} \int_{\infty}^0 u_s d\zeta = \pm \phi_s \text{ at } \zeta = 0, z = \pm b. \quad (49)$$

Mass exchange with the core, essential for the boundary conditions for pressure, occurs if the potential at the side wall varies along the wall.

$$\bar{w} = \partial_x \bar{U}_s = \partial_x \bar{\phi}_s \text{ at } \zeta = 0, z = \pm b. \quad (50)$$

The bars denote integral values along magnetic field lines.

The side layer solution is entirely prescribed if the potential at the side wall ϕ_S and the core solution is known. While the velocities u and w and the core potential ϕ have been already given in the equations (39,40 and 24), the potential at the wall is still to be determined. By using the thin wall condition at the side wall with equation (38) one obtains

$$j_z = T - \partial_x p = \mp c_S \nabla_S^2 \phi_S \text{ at } z = \pm b. \quad (51)$$

At the junctions with the Hartmann walls the potentials should be continuous, $\phi_H = \phi_S$ at $z = \pm b, y = \pm 1$. This yields for very long ducts with $\partial_{xx} \ll \partial_{yy}$ the general solution

$$\phi_S = \phi_H \mp c_s^{-1} \left(\partial_x \tilde{p} - \tilde{T} \right) \text{ at } z = \pm b. \quad (52)$$

The side layer contribution to the potential and the flow rate in the side layer $\phi_s = \pm U_s = \phi_S - \phi$ become with equation (24)

$$\phi_s(\zeta = 0) = \pm U_s = \mp c_s^{-1} \left(\partial_x \tilde{p} - \tilde{T} \right) - \partial_z \tilde{T} \text{ at } z = \pm b. \quad (53)$$

For the special case of a perfectly conducting side wall, $c_S \rightarrow \infty$, the potential along the entire side wall is uniform, $\phi_S = \phi_H$. The flow rate carried by the layer becomes simply

$$U_s = \mp \partial_z \tilde{T} \text{ for } c_S \rightarrow \infty. \quad (54)$$

This is one of the most surprising results of this paper, since for the first time a jet with $O(1)$ mass flow rate is observed at a perfectly conducting side wall. In pressure driven duct flows the core potential near the side wall is uniform along y . There, side layer jets occur only at side walls with small conductivity, when a potential profile establishes along the side wall. Here, the situation is quite different. The buoyant effect inside the channel creates a potential profile in the core near the side wall. Even if the side wall potential is uniform there exists a potential difference between the wall and the core, driving the flow rate of order one along perfectly conducting side walls. Of course, a finite conductivity of the side wall would increase this jet again. It is further interesting to notice that for the buoyancy driven convection, the flow rate carried by the side layer is not directly related to the global solution inside the core. As displayed in the equation (54) the flow rate is determined by the thermal boundary condition only. If there is a heat input e.g. by the fusion heat flux, the jet is enhanced and the heat transfer from the wall to the fluid will be promoted. If there is a heat extraction at the wall (as foreseen in actual blanket designs by separate cooling of the plasma facing first wall) the jet will reverse its direction.

4 Applications

The results derived during the last chapters are applied to the problem of a very long vertical channel typical for poloidal elements of a fusion blanket. The channel may have open ends for the case when a forced pressure difference is applied to generate an average flow though. However, one can imagine also situations when the ends are closed and the flow inside the channel is purely buoyancy driven. For the first approximation it is assumed that the channel is long enough that a fully developed regime establishes within a significantly large region along the channel axis. Fully established flow is characterized by a constant pressure gradient $\partial_x p = -K$ and vanishing derivatives $\partial_x = 0$ of all the other variables. The operators ∇_S^2 and ∇_{\perp}^2 become ∂_{yy} and ∂_{zz} , respectively.

4.1 Isothermal flows

As a first example the isothermal pressure driven flow at $T = 0$ is considered. This is nothing new (see Walker 1981 Walker (1981)) but is presented here to validate the analysis. It is assumed that the duct is symmetric with respect to $y = 0$, i.e. both Hartmann walls have equal conductivity $C_+ = C_- = C_H$. The vorticity in the core vanishes according the equation (36),

$$\omega_y = 0. \quad (55)$$

The flow is uniform in the whole core and given by the equation (39) as

$$u = K + \partial_z \phi_H. \quad (56)$$

The potential along the Hartmann wall is linear since $\partial_{zz} \phi_H = 0$ as given by equation (35). Charge conservation at the junctions between side walls and Hartmann walls $C_H \partial_z \phi_H + c_s \partial_y \phi_S = 0$ (here at $z = b, y = 1$) determine the slope and ϕ_H is obtained as

$$\phi_H = K C_H^{-1} z. \quad (57)$$

The core velocity finally becomes

$$u = K (1 + C_H^{-1}) \quad (58)$$

The flow rates carried by the side layers are

$$U_s = -c_s^{-1} \tilde{K} = \frac{1}{2} (1 - y^2) c_s^{-1} K \text{ at } z = \pm b. \quad (59)$$

If the side walls are well conducting, $c_s \rightarrow \infty$, there is no volume flux carried by the side layers. Details about the structure in the layers can be seen by considering the leading order term of the side layer solution

$$u_s \approx 16\pi^{-5/2} K c_s^{-1} \sqrt{M} e^{-\alpha \zeta} \sin \alpha \zeta \cos \beta y, \quad (60)$$

where $\beta = \pi/2$ and $\alpha = \sqrt{\pi}/2$. This solution demonstrates the magnitude of the side layer velocities, $u_s = O(K c_s^{-1} M^{1/2})$. The equation displayed above leads to the maximum value of velocity at $y = 0$, $\zeta = \sqrt{\pi}/2$, this corresponds to a distance $b - z = \sqrt{\pi/2M}$ from the wall. It shows also the possibility of partly reversed flow e.g. in the range of $2\sqrt{\pi} < \zeta < 4\sqrt{\pi}$. Towards the core as $\zeta \rightarrow \infty$ the side layer contribution vanishes exponentially.

4.2 Heat flux perpendicular to B

The non isothermal problem considered now is determined by heat conduction through a vertical channel. It is assumed that a uniform heat flux crosses the duct between the isothermal walls at $z = b$ and at $z = -b$, $\nabla T = \hat{z}$. The other walls are adiabatic. The temperature profile satisfies the conditions for symmetry with respect to $y = 0$. The temperature and the integral temperature function are given as

$$T = z, \text{ and } \tilde{T} = \frac{1}{2} (y^2 - 1) z. \quad (61)$$

Note, here the temperature scale ΔT is given by the temperature gradient times the characteristic length scale L . It is further assumed that there is no externally applied pressure gradient driving the flow; $K = 0$. It is then easy to show that for the given temperature field the velocity distribution is an odd function of z , while the potential will be an even one, $\partial_z \phi = 0$ at $z = 0$.

4.2.1 y -symmetric case

The entire problem finally becomes y -symmetric if the conductivity of both Hartmann walls are equal, $C_+ = C_- = C_H$. The potential at the Hartmann wall becomes with equation (34) $\phi_H = \frac{1}{2} C_H^{-1} z^2 + az$, when $\phi_H = 0$ is assumed at $z = 0$. The unknown integration constant $a = 0$ is obtained due to symmetry or by considering a global charge conservation $\int_0^1 j_z dy - C_H \partial_z \phi_H = 0$ at $z = b$. The Hartmann potential finally reads

$$\phi_H = \frac{1}{2} C_H^{-1} z^2. \quad (62)$$

The solution for the core potential is

$$\phi = \phi_H + \frac{1}{2} (y^2 - 1). \quad (63)$$

The core potential exhibits quite different distributions for the two limits $C_H \rightarrow \infty$ and for $C_H \ll 1$. In the first case the core potential has only a parabolic variation along magnetic field lines. In the other direction the potential is constant. This result does not correspond with the common view for MHD channel flows that for strong fields the core solution is 'projected' to the channel walls. The result, however, is obvious. The temperature gradient drives a rotational motion inside the duct. The upward flow for $z > 0$ and the downward flow for $z < 0$ induce currents in negative and positive z -direction, converging towards the center plane $z = 0$ from both sides. Charge conservation forces these currents to turn in the y -direction and to close their circuit via the Hartmann and the side walls. Along y the current density j_y increases linearly, leading to a parabolic potential distribution. The current path is plotted in figure 2. This solution is valid independently of any conductivity of the walls.

On the other hand, if $C_H \ll 1$ the variation of ϕ along z becomes much larger than the variations along y so that the Hartmann potential gives a good picture if the potential even inside the duct.

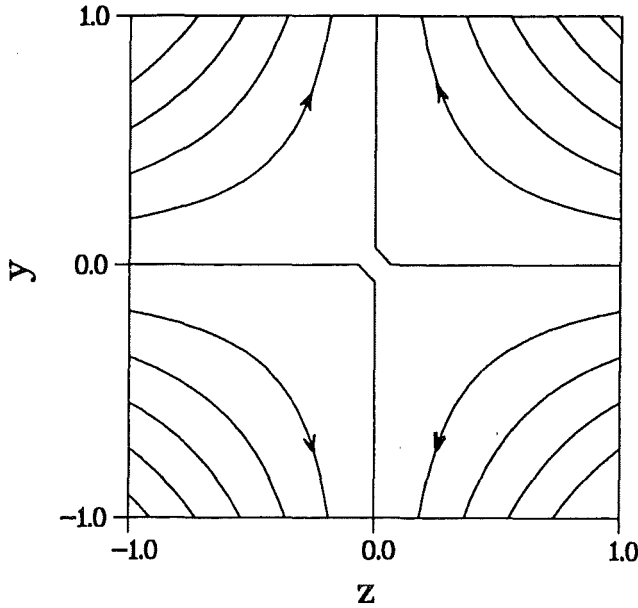


Figure 2: Path of core currents for buoyancy driven convection with $T = z$. The currents leave the core and close their circuit via the walls or the viscous layers.

The vorticity component ω_y is obtained as

$$\omega_y = C_H^{-1} + 1. \quad (64)$$

It is uniform in the whole core.

The only non-zero velocity component in the core is

$$u = (C_H^{-1} + 1) z; \quad (65)$$

the flow in the core does not depend on the y -direction, even if the potential does. For the special case of perfectly conducting walls, $C_H, c_S = \infty$ the velocity distribution in the duct is shown in figure 3 for $M = 1000$ and $b = 1$.

The most surprising result is obtained when the solution in the side layers is considered. The simplest case is that of perfectly conducting walls $C_H, c_S \rightarrow \infty$. It is known from solutions for pressure driven duct flows that there are no high-velocity jets at perfectly conducting ducts. Here, however, such jets are found as outlined in the following. For $c_S = \infty$ the side wall potential is uniform along y and identical to that of the Hartmann wall at $z = \pm b$. The viscous correction to the core solution simply becomes $\phi_s = \frac{1}{2}(1 - y^2)$ at $\zeta = 0$ and the flow rate carried by the layers is given as

$$U_s = \pm \frac{1}{2}(1 - y^2) \text{ at } z = \pm b. \quad (66)$$

This flow rate is of the same order of magnitude as the flow carried by the core. Considering now only one half of the duct, $z > 0$, supposing that all walls are perfectly conducting, leads to the result, that the total flow rate carried by this part of the duct is given by

$$\int_{-1}^1 \left(\int_0^b u dz + U_s \right) dy = b^2 + \frac{2}{3}. \quad (67)$$

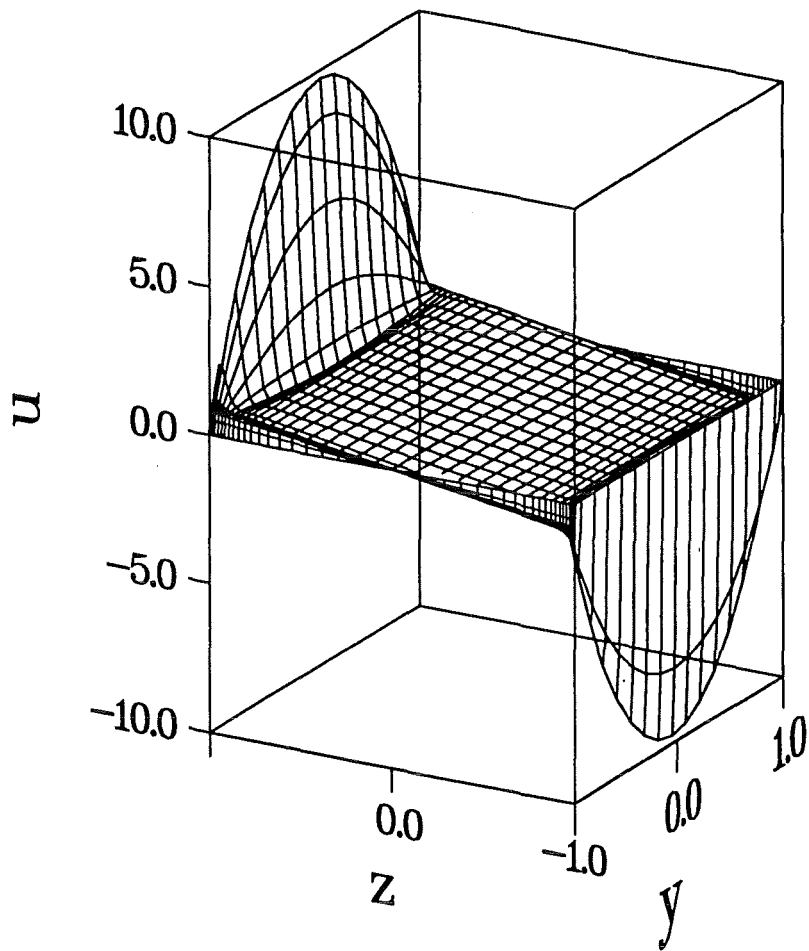


Figure 3: Buoyancy driven velocity distribution in a perfectly conducting duct with $T = z$ and $M = 1000$.

The first term on the right-hand side represents the flow in the core, the second one gives the magnitude of flow carried by the viscous side layer. This result shows clearly, that for highly conducting walls and for geometries with $b < \sqrt{2/3}$ the major part of the flow is carried by the side layer, a flow region which occupies only a minor fraction of the cross section. This may have significant implications on the design of heat transfer facilities in strong magnetic fields.

Even more severe is the case, when the side walls have finite conductivity. The current density normal to the side wall is uniform and creates along the side wall a parabolic potential distribution. $j_z = T = b = -c_S \partial_{yy} \phi_S$ at $z = b$. With $c_S < \infty$ the viscous correction to the potential and the flow rate in the layer become

$$\phi_s = U_s = \frac{1}{2} (1 - y^2) \left(\frac{b}{c_S} + 1 \right), \quad (68)$$

a value which, for small c_S , may exceed the flow in the core by orders of magnitude. As in the previous section, details about the structure in the layer can be seen by considering the leading order term of the side layer solution

$$u_s \approx 16\pi^{-5/2} \left(\frac{b}{c_S} + 1 \right) \sqrt{M} e^{-\alpha\zeta} \sin \alpha\zeta \cos \beta y, \quad (69)$$

where $\beta = \pi/2$ and $\alpha = \sqrt{\pi}/2$. This solution demonstrates the magnitude of the side layer velocities, $u_s = O\left(\sqrt{M} \left(\frac{b}{c_S} + 1\right)\right)$. For highly conducting side walls the side layer velocity is proportional to \sqrt{M} . This situation becomes even most pronounced, if the side wall conductivity is small, if $c_S \ll 1$.

Such strange behavior finds the following explanation: Inside the core the fluid is driven by buoyancy similar to the hydrodynamic case of flow in a porous medium. In the hotter part the motion is upward, in the colder part the motion is downward. Like in the porous medium, the flow suffers from strong damping which results in moderate velocities. In a porous medium the momentum of buoyant forces is balanced by viscous forces. In contrast to this, the interaction with the magnetic field transfers mechanical into electrical power. The electric power is partly dissipated within the fluid of finite electric resistance, but part of it is conducted towards the side layer region. There, it may be partly recovered. This leads to the formation of the jet-like structure in the side layers. The core acts like an electrical power generator, the side layers like MHD pumps. The direction of the jet is determined by the sign of the potential difference between the core potential near the side wall and the potential of the side wall. It is a result of the core solution and is independent of the temperature distribution within the layer itself.

4.2.2 Non y -symmetric case

An interesting situation occurs if the channel is not symmetric with respect to $y = 0$, say one Hartmann wall is better conducting than the other; $C_- \gg C_+$. Under this assumption the potential at the better conducting wall is uniform compared with the other potentials. For convenience one can choose the level of potential at this wall to $\phi_- = 2\partial_z \bar{T} = 2$ at $y = -1$. The potential at the other Hartmann wall at $y = 1$ then is

calculated by the use of equation (34)

$$C_+ \partial_{zz} \phi_+ - \frac{1}{2} \phi_+ = 0, \quad (70)$$

which leads to

$$\phi_+ = \phi_c \frac{\cosh \frac{z}{\sqrt{2C_+}}}{\cosh \frac{b}{\sqrt{2C_+}}}. \quad (71)$$

The integration constant ϕ_c introduced above is the potential at the corner, at $z = b$, $y = 1$. It is determined by considering the solution for the potential at the side wall. The current entering the side wall is $j_z = T = b$ according to equations (38). This current enters the side wall and creates there a potential distribution $b = -\partial_{yy} \phi_S$ (see equation (51)). The solution of this equation finally determines the potential at the corner by the matching conditions for the Hartmann and the side wall potentials $\phi_+ = \phi_S = \phi_c$, $C_+ \partial_z \phi_+ + c_S \partial_y \phi_S = 0$ at $z = b$, $y = 1$ and $\phi_S = \phi_- = 2$ at $z = b$, $y = -1$.

$$\phi_c = 2 \frac{c_s + b}{c_s + \sqrt{2C_+} \tanh \frac{b}{\sqrt{2C_+}}}. \quad (72)$$

These results already show the following interesting limits: If the wall at $y = 1$ is well conducting the potential will find a parabolic distribution along z . On the other hand, if the conductance is poor there exists a possibility for a new type of exponential side layers with a width of the order $C_+^{1/2}$. Before a detailed discussion of this result the velocity in the core is calculated using the equation (39).

The core velocity is given by

$$u = z + (1 + y) \frac{\phi_c}{2\sqrt{2C_+}} \frac{\sinh \frac{z}{\sqrt{2C_+}}}{\cosh \frac{b}{\sqrt{2C_+}}}. \quad (73)$$

Even if the temperature is constant along y , the velocity profile does not reflect this behavior. The velocity is non-uniform in this direction. The most interesting velocity distribution is obtained for moderate conductivity of the Hartmann wall; say for $C_+^{1/2} \ll 1$. Under this assumption the velocity profile in the core becomes

$$u \approx z \mp \frac{1}{2} (1 + y) \frac{\phi_c}{2\sqrt{2C_+}} \exp \frac{|z| - b}{\sqrt{2C_+}}, \text{ for } z \lesssim 0. \quad (74)$$

The flow rate carried by the convective motion in the hotter part of the core is obtained as

$$\int_0^b \int_{-1}^1 u dy dz = b^2 + \frac{1}{2} \phi_c \left(1 - \frac{1}{\cosh \frac{b}{\sqrt{2C_+}}} \right). \quad (75)$$

The results described above have show the possibility of a second type of MHD side layer. These side layers are a part of the inviscid core. Their thickness scales with the conductivity of the poor conducting Hartmann wall as $C_+^{1/2}$. Within these inviscid layers the velocity is a linear function along magnetic field lines. This is in contrast to the

viscous side layers where the velocity profile has a parabolic shape along the side wall. Similar layers have been mentioned already by Walker (1981) for pressure driven duct flows with variable rectangular cross section. While Walker uses the terms *outer* and *inner* layers motivated by the mathematical procedure, in the present paper the terms *inviscid* and *viscous* layers are used, respectively to characterize the particular physics in each layer.

One can imagine situations when almost all core flow is carried by these layers, depending on the parameters used for the conductivity of the Hartmann wall. For $C_+^{1/2} \ll 1$, the inviscid layer may carry a significant fraction of the total flow. This fraction is further called $2\bar{U}_i$ and reads

$$2\bar{U}_i = \phi_c = 2 \frac{c_s + b}{c_s + \sqrt{2C_+}} \text{ for } \sqrt{C_+} \ll 1. \quad (76)$$

The ratio of flow carried by the inviscid layer to the flow carried by the rest of the core may become really large if c_s and $\sqrt{C_+}$ are small compared with the half width b of the duct.

In addition the viscous side layers are still present. It is now interesting to compare the flow rate in the inviscid layer with the flow rate in the viscous layer. It can be shown that the flow rate in the viscous layer is the same as for the y -symmetric case discussed one section above, $2\bar{U}_s = \frac{2}{3} \left(\frac{b}{c_s} + 1 \right)$. For the comparison of flow rates it is assumed that the Hartmann wall and the side wall are poor conductors, $c_s, \sqrt{C_+} \ll 1$. Then, the ratio of flow carried by the inviscid and the viscous layer becomes

$$\frac{\bar{U}_i}{\bar{U}_s} = \frac{3}{1 + \frac{\sqrt{2C_+}}{c_s}}. \quad (77)$$

Depending on the parameters one can imagine situations when most flow is carried by the uniform core or when most flow is carried by the viscous and the inviscid layers. However, the inviscid layer will never carry more than 3 times the flow of the viscous layer. These examples should shortly outline the high sensitivity of the flow distribution inside the cross section to the electrical boundary conditions.

One result of those described above is displayed in figure 4. for $C_+ = 0.05$, $c_s = 1$. $M = 1000$.

The inviscid layers become clearly visible near the side walls. The magnitude of velocity in the core is small near the highly conducting Hartmann wall at $y = -1$ but most pronounced near the poor conducting Hartmann wall. The non-symmetry with respect to $y = 0$ can be also seen by considering the current path in the core. For a low conductivity of the upper Hartmann wall most currents leaving the core enter the lower, perfectly conducting Hartmann wall. They close their circuit via the conducting side walls and enter the core again near $z = \pm 1$. Only a minor fraction takes the other path via the high resistance upper Hartmann wall. Increasing the conductivity of the upper wall increases this fraction and finally a symmetric situation as shown in figure 2 is reached when $C_+ = \infty$.

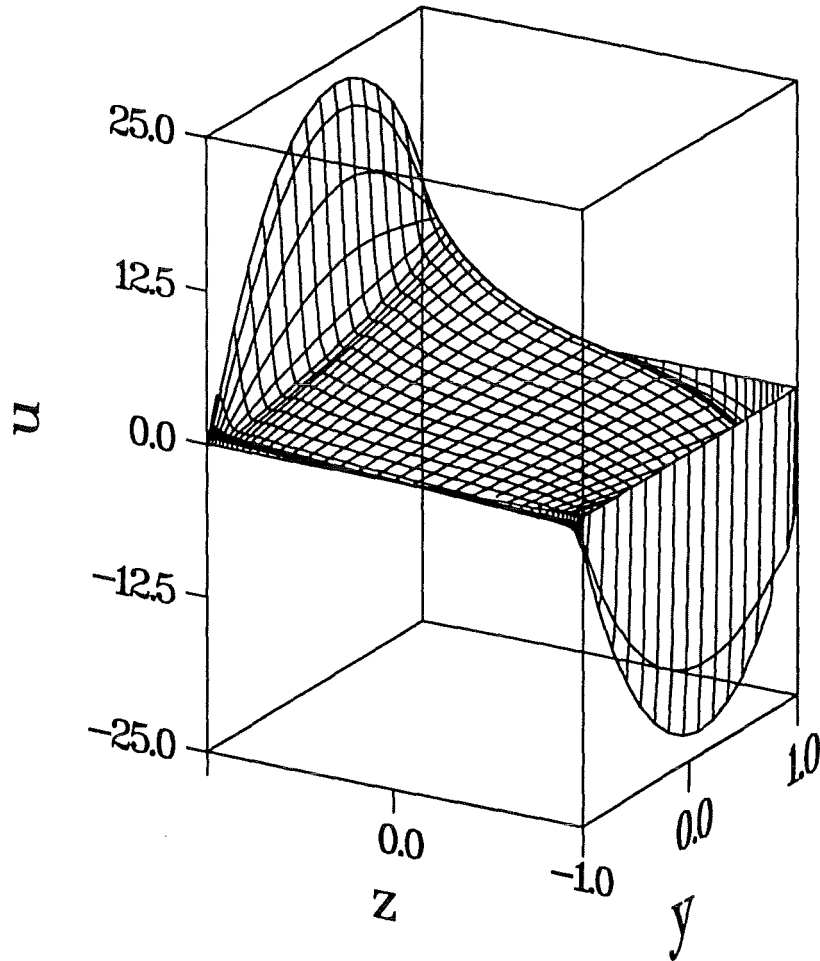


Figure 4: Velocity distribution for buoyancy driven convection with $T = z$ and $M = 1000$. The lower Hartmann wall is perfectly conducting, $C_- = \infty$; the other conductivities are $C_+ = 0.05$, $c_S = 1$. One can observe the thicker inviscid layers near $z = \pm b$.

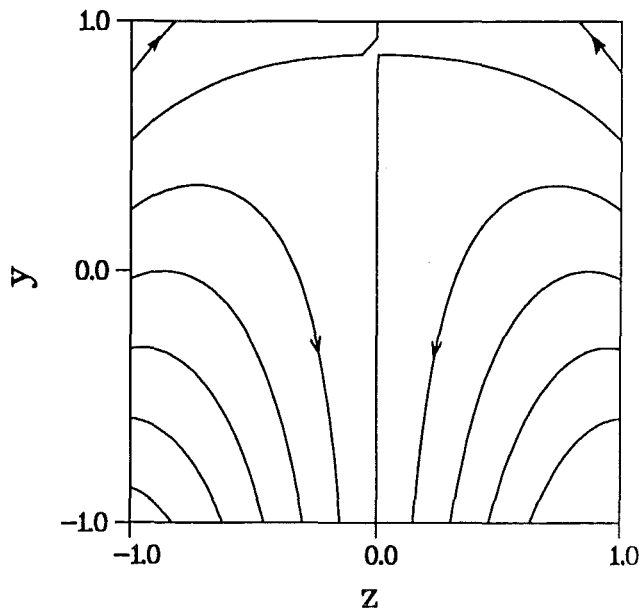


Figure 5: Path of core currents for buoyancy driven convection with $T = z$ and $M = 1000$. The lower Hartmann wall is perfectly conducting, $C_- = \infty$; the other conductivities are $C_+ = 0.05$, $c_S = 1$. The currents leave the core and close their circuit preferentially via the highly conducting walls at $y = -1$ and at $z = \pm 1$. As the upper Hartmann wall conductivity increases the current pattern approached that of the symmetric case as already shown.

4.3 Heat flux aligned with \mathbf{B}

For the second example the heat flux is turned by is 90° in the horizontal plane. The temperature gradient is now aligned with the magnetic field, $\nabla T = \hat{y}$ and the temperature and the temperature function become

$$T = y, \quad \tilde{T} = \frac{1}{6}(y^3 - 1). \quad (78)$$

The conductivity of both Hartmann walls are assumed to be equal, $C_+ = C_- = C_H$. The potential at the Hartmann wall at $y = 1$ is determined by equation (34). The temperature field is an odd function with respect to $y = 0$. This behavior is reflected on the potentials $\phi_+ = -\phi_-$. The solution for the potential ϕ_+ becomes

$$\phi_+ = \phi_c \frac{\sinh \frac{z}{\sqrt{C_H}}}{\sinh \frac{b}{\sqrt{C_H}}}, \quad (79)$$

when $\phi_+ = 0$ is assumed at $z = 0$. The integration constant ϕ_c introduced above is the potential at the corner, at $z = b$, $y = 1$. The core potential finally reads

$$\phi = \phi_+ y. \quad (80)$$

Side layer jets occur only for side walls with a finite conductivity $c_S < \infty$. The equation determining the potential at the side wall (51) is $j_z = y = -c_S \partial_{yy} \phi_S$.

$$\phi_S = \phi_c y + \frac{y - y^3}{6c_S}. \quad (81)$$

Continuity of electric currents at the corner finally determines ϕ_c as

$$\phi_c = \frac{1}{3} \frac{1}{c_s + \sqrt{C_H} \coth \frac{b}{\sqrt{C_H}}}. \quad (82)$$

If no external pressure difference is driving an average flow rate, the velocity is determined using $u = T + \partial_z \phi$.

$$u = y (1 + \partial_z \phi_+) \quad (83)$$

and the velocity inside the core becomes

$$u = y \left(1 + \frac{\phi_c}{\sqrt{C_H}} \frac{\cosh \frac{z}{\sqrt{C_H}}}{\sinh \frac{b}{\sqrt{C_H}}} \right). \quad (84)$$

The solution far away from the side walls takes, as expected, the same values as a flow between two vertical flat, infinite Hartmann walls. (see e.g. Blüms et al. (1987) p.167). The present result includes now the effects of a finite extend of the duct in the z -direction. It is remarkable that even if the temperature field is uniform along z , the velocity field may exhibit the strongest variations in this direction. Thin, high-velocity side layer jets are formed, which may carry a significant fraction of the total flow rate. As an example the flow in a duct with $M = 1000$, $C_H = 0.05$ and $c_s = 0.1$ is displayed in figure 6. The flow pattern is qualitatively similar to that obtained by Ben Hadid and Henri (1997) by a fully numerical simulation of MHD flow in a geometry related to a horizontal Bridgman device for crystal growth applications. Even if their electrical boundary conditions and the orientation of the magnetic field and the temperature gradient are different to the problem considered here, the main physical mechanisms should be the same. The main reason for a good qualitative agreement may be that the temperature gradient and the direction of the magnetic field are mutually perpendicular in their paper as well as in the present work. They had a temperature gradient aligned with the ducts axis which was oriented perpendicular to the direction of gravity. Here the axis is aligned with gravity, normal to the temperature gradient. It should be a straight forward exercise to recast their problem in the present notation, extending their results for nonconducting ducts to geometries with arbitrary conductivities. Moreover, the present formulation gives the analytical relationship between the physical variables with no upper restriction on the Hartmann number while numerical solutions are currently restricted to Hartmann numbers in the range of 10^2 .

The total flow rate in the hotter part of the duct, for $y > 0$ is obtained as

$$\int_0^1 \left(\int_{-b}^b u dz + U_s \right) dy = b + \phi_c + \frac{1}{12c_s}. \quad (85)$$

The first two terms on the right-hand side in this equation correspond to the flow rate carried by the core, the second gives the flow rate of the inviscid layer, and the last one gives the flow carried by the viscous layer. If the conductivities of the walls are small, say $c_s, \sqrt{C_+} \ll 1$ all flow is carried by the viscous and the inviscid layers. The rest of the core is almost stagnant. The flow rate in both types of side layers may exceed that

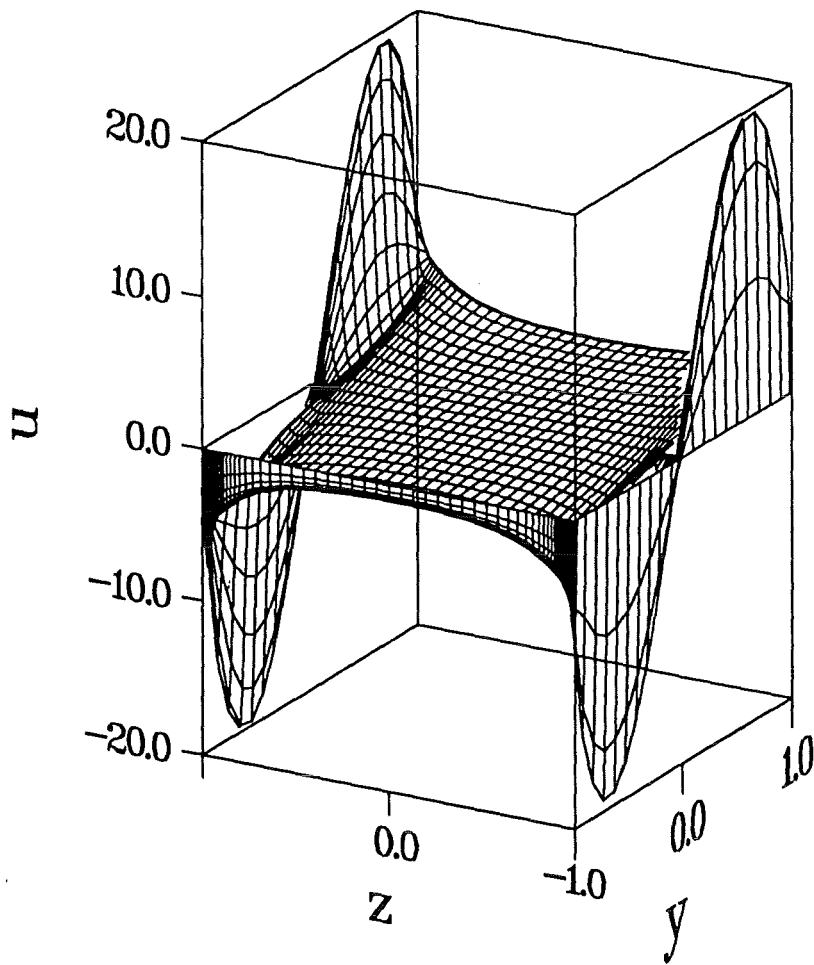


Figure 6: Velocity distribution for buoyancy driven convection with $T = y$ and $M = 1000$. The conductivities of the walls are $C_H = 0.05$, $c_s = 0.1$. One can observe the thicker invicid layers which are part of the core. Along the side walls the viscous layers exhibit strong velocity jets.

of the rest of the core if c_s becomes small or ϕ_c becomes large. The flow distribution between the two layers is determined by

$$\frac{\int_0^1 U_i dy}{\int_0^1 U_s dy} = \frac{4}{1 + \frac{\sqrt{c_+}}{c_s}}. \quad (86)$$

The structure of the viscous side layer remains similar as for the case when the heat flux is perpendicular to the side walls, except that the $\cos(\beta y)$ function is replaced by $\sin(\beta y)$ and some coefficients change their values. The leading order term of the side layer solution is

$$u_s \approx 2\pi^{-5/2} \frac{\sqrt{2M}}{c_s} e^{-\alpha\zeta} \sin \alpha \sin \beta y, \quad (87)$$

where now $\beta = \pi$ and $\alpha = \sqrt{\pi/2}$. This solution behaves similar along ζ as that in the previous section. Along y the flow varies according to the odd function $\sin \beta_1 y$. There is a flow in the x -direction for $y > 0$ and a reversed flow for $y < 0$ in the same layer.

The electric currents which oppose the fluid motion in the core have to close via the side wall. Part of these currents flow from the front half of the side wall to the rear half, from $y > 0$ to $y < 0$. Another part leaves the side wall at $y = \pm 1$ and enters the Hartmann walls or vice versa. For poor conducting walls the currents are limited by the resistance in the walls. The breaking effect by Lorentz forces is reduced and buoyant effects may create large velocities. If one of these walls is perfectly conducting, ϕ_c , the potential at the corner vanishes. The currents and the flow rate in the core become $O(1)$ since the only current limiting resistance is that of the fluid itself. The current path for the example discussed above is shown in figure 7.

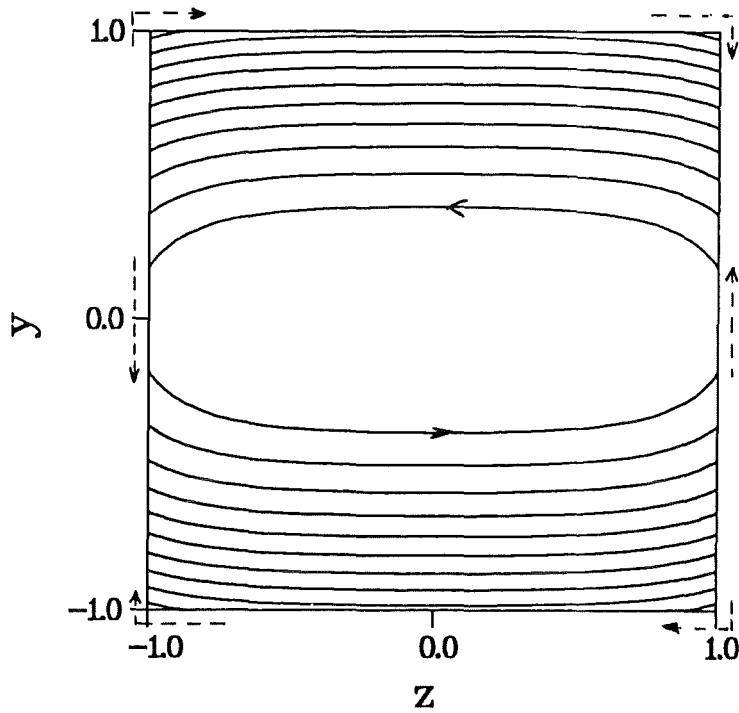


Figure 7: Current path for buoyancy driven convection with $T = y$ and $M = 1000$. The conductivities of the walls are $C_H = 0.05$, $c_s = 0.1$. The currents induced in the core partly enter the side walls along which they close from $y > 0$ to $y < 0$. The other part leaves the side wall and enters the Hartmann walls at $y = \pm 1$, $z = \pm b$. This part of currents is distributed to the core across the Hartmann layers and is responsible for the formation of the inviscid part of the velocity jets.

5 Conclusions

The buoyancy driven laminar MHD flow in long vertical channels of rectangular cross section has been investigated. Of particular interest for the present analysis was the horizontal orientation of the applied strong magnetic field, parallel to one pair of duct walls. Such geometries are typical for fusion applications in self-cooled or in separately cooled liquid metal blankets.

The basic equations have been used in nondimensional form with a velocity scale proportional to the ratio of buoyant forcing to magnetic damping Gr/M^2 . With this representation the equations become uniquely valid with M as the only parameter. The wall conductance ratio c enters the problem via the boundary conditions as a second parameter. The magnetoconvective flow has been calculated using the inductionless approximation by applying asymptotic methods for high Hartmann numbers M . The integral temperature function \bar{T} allows a compact representation of the analysis in closed form for any temperature distribution.

One can identify the commonly known flow subregions: the inviscid core, where buoyant forces are balanced by Lorentz forces, the Hartmann layers with thickness of the order M^{-1} with a balance between Lorentz - and viscous forces, the side layers with thickness proportional to $M^{-1/2}$ caused by a balance of the potential difference between the core and the side walls with the induced potential of the high velocity jets. In addition inviscid layers near the side walls are found which are part of the core and scale in thickness as $c^{1/2}$. The later ones are caused by a current exchange between the Hartmann walls and the core across the Hartmann layers. Nonzero currents through the Hartmann layers are a source of vorticity and responsible for large velocity gradients in these regions (compare e.g. Böhler and Molokov (1994)). In the isothermal case the results reduce to the well-known solution for pressure driven duct flows. Results for pure buoyancy driven flows are presented for the cases of a uniform heat flux through the side walls, $T = z$ or through the Hartmann walls, $T = y$.

The first example of a buoyant flow is most closely related to applications in fusion engineering, where the major heat exchange is via a walls aligned with the magnetic field, called the *first wall*. In order to analyze the results quantitatively, the upward flow rate in the hotter part of the duct is considered. For walls relatively well conducting compared with the conductivity of the viscous layers, $M^{-1} \ll C_H, c_S^2 \ll 1$, the flow rates carried by the core and those carried by the viscous side layers become proportional to b^2/C_H and to $\frac{2}{3}b/c_S$, respectively. All currents induced in the core have to close their path via the Hartmann walls. The conductivity of these walls is still small compared to unity and thus the walls give an upper limit for the currents and Lorentz forces by their Ohmic resistance. As a result, the flow rate in the core is proportional to C_H^{-1} a value which may exceed that of order one, observed in perfectly conducting ducts. Moreover, high-velocity jets are formed along the walls at which the heat is transferred. These viscous jets carry a volume flux proportional to c_S^{-1} , favorable for heat transfer. For the case of perfectly conducting walls, $C_H, c_S = \infty$, the flow in the core becomes $O(1)$. The most surprising result, however, is the fact that even for perfectly conducting side walls a jet with order one flow rate remains. The velocities are proportional to $M^{1/2}$ times the wall heat flux into the channel. Jets along perfectly conducting walls are not observed in classical pressure driven duct flow problems. Here, for the first time, such

jets are found. Even if the velocities in the core are moderate those along perfectly conducting side walls are large. These results should stipulate again discussions about the feasibility of poloidal self-cooled fusion blankets.

In currently investigated blanket concepts a number of ducts are combined in parallel to form a torus segment. Some of these ducts have walls towards an insulating surrounding, others face conducting neighboring channels. This leads to non-symmetric conditions for the flow inside those ducts, even if the thermal conditions suggest symmetry. To analyze the effect of non-symmetry an extreme case has been chosen where one Hartmann wall is assumed to be perfectly conducting. For the same temperature distribution as discussed just above, $T = z$, the velocity in the core no longer remains uniform along magnetic field lines. The core itself forms layers near the side walls, here called the inviscid layers, in which a large amount of flow may be carried. The thickness of these layers is proportional to $C_+^{1/2}$, the finite conductivity of the other Hartmann wall. In addition to these inviscid layers the viscous ones are still present.

The third example discussed does not have a direct relation with fusion applications since the heat flux enters or leaves the channel via the Hartmann walls, $T = y$. For this temperature distribution one finds a linear velocity profile in the core along the magnetic field lines, $u = y$, far from the side walls. The result is in accordance with known solutions Blüms et al. (1987). Near the side walls, again inviscid layers with thickness proportional to $C_H^{1/2}$ and viscous layers of thickness of the order $M^{-1/2}$ are present. Both layers may carry the major fraction of flow rate depending on the combination of the conductivity of the Hartmann and the side walls.

The examples for which results are displayed in the present paper already show the large variety of possible flow configurations. Examples including internal heating are not included in this work but covered by the present analysis. The analysis is performed here for long vertical channels in the frame of fusion applications. Nevertheless, it should be possible to apply the present ideas to other problems like the flow in a long horizontal Bridgman configuration for crystal growth where similar phenomena are observed.

References

- Albousière, T., Garandet, J. and Moreau, R. (1993). Buoyancy-driven convection with a uniform magnetic field. part 1. asymptotic analysis, *Journal of Fluid Mechanics* **253**: 545–563.
- Albousière, T., Garandet, J. P. and Moreau, R. (1996). Asymptotic analysis and symmetry in MHD convection, *Physics of Fluids* **8**(8): 2215–2226.
- Ben Hadid, H. and Henri, D. (1997). Numerical study of convection in a horizontal Bridgeman configuration under the action of a constant magnetic field. Part 2. three-dimensional flow, *Journal of Fluid Mechanics* **333**: 57–83.
- Ben Hadid, H., Henri, D. and Kaddeche, S. (1997). Numerical study of convection in a horizontal Bridgeman configuration under the action of a constant magnetic field. Part 1. two-dimensional flow, *Journal of Fluid Mechanics* **333**: 23–56.
- Blūms, E., Mikhailov, Y. and Ozols, R. (1987). *Heat and mass transfer in MHD flows*, World Scientific Publishing Co. Pte. Ltd.
- Bühler, L. and Molokov, S. (1994). Magnetohydrodynamic flows in ducts with insulating coatings, *Magnetohydrodynamics* **30**(4): 439–447.
- Garandet, J., Albousière, T. and Moreau, R. (1992). Buoyancy driven convection in a rectangular enclosure with a transverse magnetic field., *Int. J. Heat Mass Transfer* **35**(4): 741–748.
- Hjellming, L. N. and Walker, J. S. (1987). Melt motion in a Czochralski crystal puller with an axial magnetic field: motion due to buoyancy and thermocapillarity, *Journal of Fluid Mechanics* **182**: 335–368.
- Hjellming, L. N., Tolley, P. A. and Walker, J. S. (1993). Melt motion in a Czochralski crystal puller with a non-uniform axisymmetric magnetic field: isothermal motion, *Journal of Fluid Mechanics* **249**: 1–34.
- Khine, Y. and Walker, J. (1994). Thermocapillary convection in a cylinder with a strong non-uniform axisymmetric magnetic field, *Journal of Fluid Mechanics* **276**: 369–388.
- Ma, N. and Walker, J. S. (1995). Liquid-metal buoyant convection in a vertical cylinder with a strong vertical magnetic field and with nonaxisymmetric temperature, *Physics of Fluids* **7**(8): 2061–2071.
- Ma, N. and Walker, J. S. (1996a). Buoyant convection during the growth of compound semiconductors by the liquid-encapsulated Czochralski process with an axial magnetic field and with non-axisymmetric temperature, *Journal of Fluids Engineering* **118**(8): 155–159.

- Ma, N. and Walker, J. S. (1996b). Magnetic damping of buoyant convection during semiconductor crystal growth in microgravity. Continuous random g-jitters, *Physics of Fluids* **8**(4): 944–953.
- Möbner, R. (1996). Dreidimensionale numerische Simulation von Naturkonvektionsströmungen unter dem Einfluß von Magnetfeldern, *Technical Report FZKA 5748*, Forschungszentrum Karlsruhe.
- Takashima, M. (1994). The stability of natural convection in a vertical layer of electrically conducting fluid in the presence of a transverse magnetic field., *Fluid Dynamics Research* **14**: 121–134.
- Walker, J. S. (1981). Magnetohydrodynamic flows in rectangular ducts with thin conducting walls, *Journal de Mécanique* **20**(1): 79–112.